The electronic spin state of diradicals obtained from the nuclear perspective: the strange case of Chichibabin radicals

Gabriel Moise,*†,(a) Saleta Fernández,†,(b) Kit Joll,(a),(c) Mikhail Vaganov,(a) Fátima García,(b) Christiane R. Timmel,(c) Diego Peña,(b) and Arzhang Ardavan(a)

(a) *Centre for Advanced Electron Spin Resonance, The Clarendon Laboratory, Department of Physics, University of Oxford, Parks Road, Oxford, United Kingdom, OX1 3PU.*
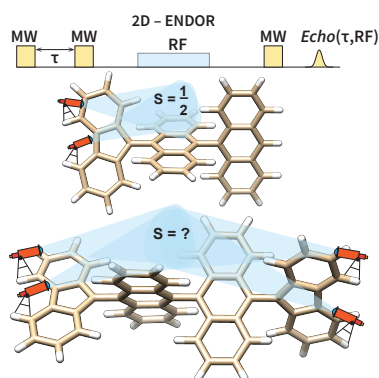
(b) *Centro Singular de Investigación en Química Biolóxica y Materiais Moleculares, C/ Jenaro de la Fuente s/n (esquina Avda. Mestre Mateo), Campus Vida, Universidade de Santiago de Compostela, Santiago de Compostela, Spain, 15782.*

(c) *Centre for Advanced Electron Spin Resonance, Inorganic Chemistry Laboratory, University of Oxford, South Parks Road, Oxford, United Kingdom, OX1 3QR.*

† *These authors contributed equally.*

* *Corresponding authors: arzhang.ardavan@physics.ox.ac.uk; gabriel.moise@physics.ox.ac.uk; diego.pena@usc.es*

Abstract. With a view towards the development of molecular spintronics, non-linear optics, and qubits, a great amount of research effort aims to establish the factors which govern the spin classification of diradicals. Electron spin resonance (ESR) is an indispensable tool for such research. However, in some cases, the mere presence of an ESR spectrum is insufficient to ascertain that the presumed diradical is indeed a triplet state. In a comparative case study of a Chichibabin diradical and a monoradical analogue, we show how the signals from different spin states present in liquid solutions of these species may be disentangled. Ultimately, the correct spin classification depends on ESR techniques which probe the spin quantum number directly. In this work, electron nuclear double resonance experiments reveal that the nuclei provide the clearest experimental probe of the electronic spin configuration.

Contents

1 Introduction

Polycyclic aromatic hydrocarbons (PAHs) represent a family of organic compounds formed by the fusion of aromatic rings.[1-3] In this work, we focus our attention on the open-shell subclass of PAHs with one/two unpaired electrons. A variety of studies show that the presence of unpaired electrons in these species leads to a number of interesting properties such as: two photon absorption enhancement,[4] singlet fission,[5] interesting chiroptical,[6,7] or amphoteric redox behaviour.[8] These properties make open-shell PAHs attractive for applications in the fields of materials science, spintronics, and quantum computing.[9-13] Accordingly, the design and synthesis of open-shell PAHs is an active field of research.[14-19] Among the many open-shell PAHs synthesised to date, derivatives of Chichibabin's hydrocarbons stand out due to their stability under ambient conditions.[20] Particular examples of such stable Chichibabin radicals are those bearing anthracene units as the central core.[21-23]
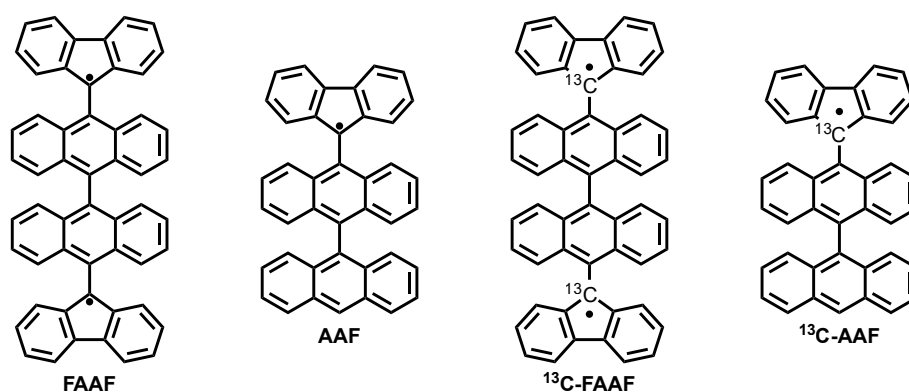
Figure 1: Structures of radical species studied in this work. The species are labelled as follows: **F** represents a fluorenyl fragment and **A** denotes an anthryl fragment.

When it comes to characterising the properties of open-shell PAHs, electron spin resonance (ESR) is a valuable technique because it directly probes the electron spin density of paramagnetic molecules. In its most popular implementation, continuous-wave ESR (cwESR) is used as a simple analytical tool for ascertaining that a particular compound is paramagnetic. However, this question becomes more complicated when it comes to determining the spin states of compounds with more than one unpaired electron. For example, consider an organic diradical: the absence of cwESR signals is often attributed to the diamagnetic singlet state, while the presence of a cwESR signal is linked to the triplet state. However, the mere existence of a non-zero cwESR spectrum is not sufficient to conclude that the observed paramagnetic species is the triplet state of the diradical. In fact, from a quantum mechanical perspective, the situation is worse: if the spin Hamiltonian of the diradical does not commute with $\hat{S}^2$ (the square of the total electronic spin operator), the system may exist in a quantum state which is neither singlet nor triplet. Consider the uncertainty relation: $\Delta S^2 \Delta E \geq \frac{1}{2} \left| \left\langle \left[\hat{H}, \hat{S}^2 \right] \right\rangle \right|$, where ΔS^2 and ΔE are the uncertainties in S^2 and energy, respectively. This relation implies that it is not generally possible to specify the energy and total spin simultaneously and with arbitrary precision. Hence, the correct classification of the spin state of diradicals requires a detailed characterisation of the various interactions present in the spin Hamiltonian. In particular, one requires pulse ESR experiments which can measure the total spin quantum number directly.

In this work, we present a continuous-wave, pulse ESR, and electron-nuclear double resonance (ENDOR) case study of the Chichibabin radicals shown in figure 1. These systems serve as model compounds for the wider class of open-shell PAHs. Given the above mentioned intricacies of classifying the spin states of diradicals, the focus of the study is on understanding the behaviour of liquid solutions of the **FAAF** molecule, which was previously investigated by Zeng et al.[21] The **AAF** monoradical, which benefits from a well-defined electronic spin-1/2, will serve as an essential reference point for the ESR data obtained for **FAAF**. Additionally, the ^{13}C substituted derivatives benefit from larger hyperfine couplings which facilitate the deconvolution of the cwESR spectra.

The diradical **FAAF** was synthesized following the procedure reported by Zeng et al. (Figure 2).[21] Specifically, 10,10'-dibromo-9,9'-bianthracene (**1**) was treated sequentially with n-BuLi and fluorenone (**2a**) to yield diol (**3a**). Then, reaction of compound **3a** with SnCl$_2$ afforded the diradical **FAAF**, which is stable enough to be purified by column chromatography and isolated under ambient conditions. A similar synthetic procedure was used for the preparation of monoradical **AAF**, from 10-bromo-9,9'-bianthracene (**4**). In this case, **AAF** was isolated in a 52% yield by reaction of alcohol **5a** with SnCl$_2$.[24] For the preparation of isotopically labelled radicals ^{13}C−**FAAF** and ^{13}C−**AAF**, it was first necessary to prepare the labelled fluorenone **2b** (see SI for details). Then, the corresponding isotopically labelled radicals were obtained following the same procedure as for the preparation of **FAAF**.
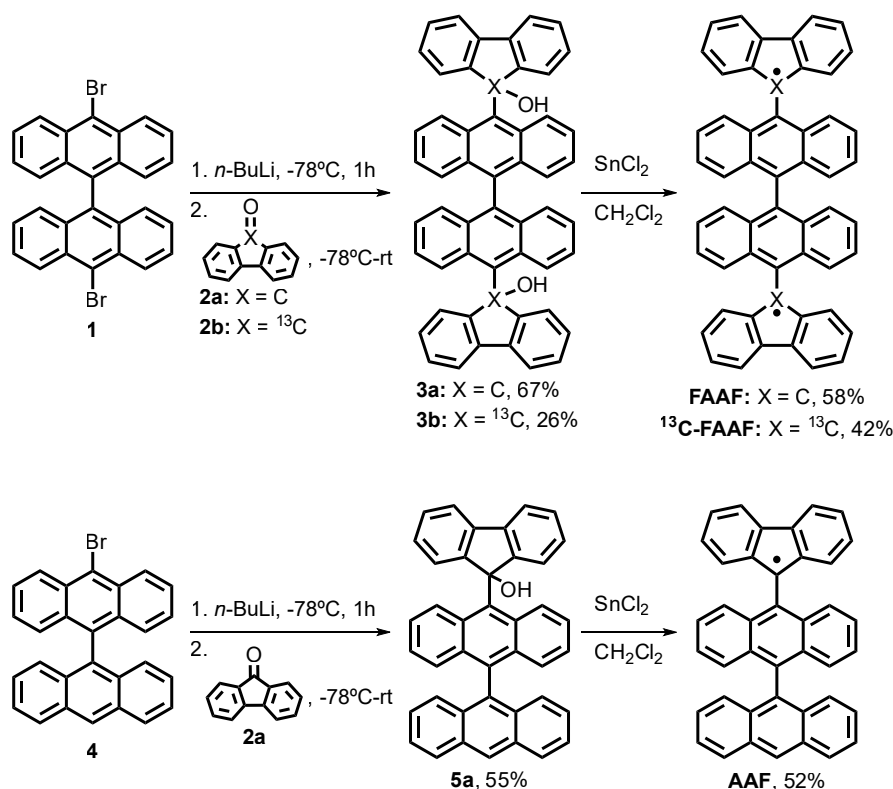
Figure 2: Synthesis of diradicals **FAAF** (top) and monoradicals **AAF** (bottom).

2 Results and Discussion

2.1 Continuous-wave ESR

The initial discussion will focus on the room temperature cwESR results obtained for the monoradical reference system, **AAF**, in liquid solutions of dichloromethane. The experimental and simulated cwESR spectra are shown in figure 3. A compilation of simulation parameters is shown in table 1. Complete details regarding acquisition, sample preparation, and data analysis are given in the SI.

FAAF – doublet		FAAF – triplet		AAF	
Parameter	Value	Parameter	Value	Parameter	Value
$a_{\text{iso}}(1\times{}^{13}\text{C})$	54.3	$a_{\text{iso}}(2\times{}^{13}\text{C})$	27.1 ± 0.27	$a_{\text{iso}}(1\times{}^{13}\text{C})$	57.10
$a_{\text{iso}}(4\times{}^{1}\text{H})$	10.01 ± 0.40	$a_{\text{iso}}(8\times{}^{1}\text{H})$	4.80 ± 0.45	$a_{\text{iso}}(4\times{}^{1}\text{H})$	10.25 ± 0.26
$a_{\text{iso}}(2\times{}^{1}\text{H})$	2.27 ± 0.23	$a_{\text{iso}}(2\times{}^{1}\text{H})$	1.60 ± 0.65	$a_{\text{iso}}(2\times{}^{1}\text{H})$	2.37 ± 0.15
$a_{\text{iso}}(2\times{}^{1}\text{H})$	1.81 ± 0.12			$a_{\text{iso}}(2\times{}^{1}\text{H})$	1.80 ± 0.06
σ_L/mT	0.06	σ_L/mT	0.06	σ_L/mT	0.04
σ_G/mT	0.03	σ_G/mT	0.03	σ_G/mT	0.03
g-factor	2.0028	g-factor	2.0029	g-factor	2.0028

Table 1: CwESR simulation parameters: isotropic hyperfine couplings (a_{iso}), Lorentzian and Gaussian broadenings (FWHM: σ_L and σ_G), and isotropic g-factors. For the unlabelled **FAAF** spectrum, we find a relative doublet/triplet weighting of 77%/23%. For the ^{13}C labelled **FAAF** spectrum, the weighting was approximately 50% for both components.

The room temperature spectra of the ^{13}C labelled and unlabelled **AAF** systems are typical of organic radicals with transitions centred around $g_e \approx 2.0023$. The largest hyperfine splitting in panel (a) is caused by couplings to

four approximately equivalent protons with a Fermi contact interaction $a_{iso} \approx 10\,\mathrm{MHz}$. For the labelled system in panel (b), a Fermi contact interaction of $\sim 57\,\mathrm{MHz}$ to $^{13}\mathrm{C}$ causes a 'doubling' of the spectrum. These hyperfine parameters are broadly consistent with the Density Functional Theory (DFT) results shown in the SI. The DFT calculation predicts a spin density localised primarily on the fluorenyl (**F**) side of the molecule with minimal leakage onto the anthryl fragments. According to DFT, the four $10\,\mathrm{MHz}$ $^1\mathrm{H}$ couplings belong to the *ortho* and *para* protons relative to the carbon atom with the largest spin density – *i.e.* marked with a dot in figure 1 (see also ENDOR discussion below). The next largest DFT predicted couplings correspond to the *meta* protons, and are represented in the spectral simulations as the two additional sets of two protons with couplings of ca. $2\,\mathrm{MHz}$. It is important to highlight the remarkable quality of the simulations of the **AAF** spectra in panels (a) and (b) of figure 3. The RMSD of the best fit is $\sim 0.5\%$. Such a good fit is not possible for the spectra of **FAAF** in a *single component* simulation. The reason why single-component simulations fail for **FAAF** can be most easily understood by visual inspection of the data in panel (d). A hyperfine coupling to two equivalent $^{13}\mathrm{C}$ nuclei ought to produce a spectrum which is the convolution of the unlabelled spectrum – panel (c) – with a $1 : 2 : 1$ splitting pattern caused by the larger $^{13}\mathrm{C}$ couplings. Instead, the spectrum in panel (d) appears to be an overlap of the spectrum in panel (b) with another spectrum which has the expected $1 : 2 : 1$ $^{13}\mathrm{C}$ splitting pattern.
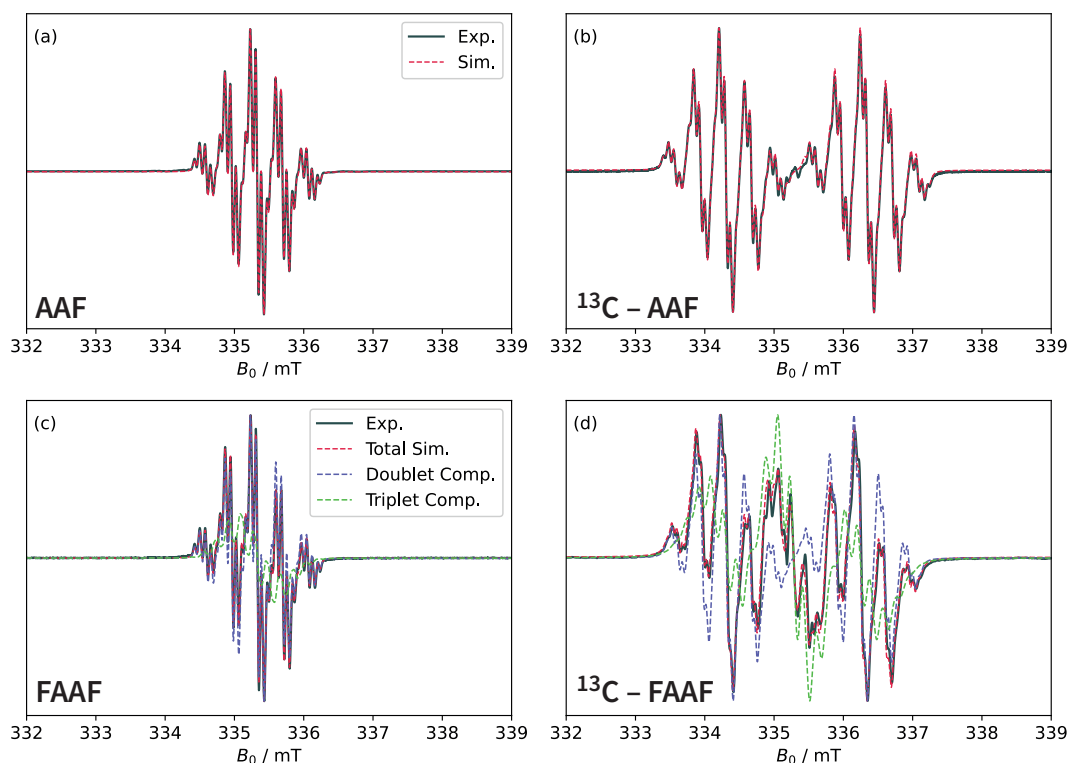

Figure 3: CwESR data and simulations obtained at room temperature in liquid solutions using dichloromethane as the solvent. (a) and (b) correspond to the **AAF** system with and without $^{13}\mathrm{C}$ labelling, as indicated. (c) and (d) correspond to the **FAAF** system with and without $^{13}\mathrm{C}$ labelling. The simulations of the **FAAF** spectra are comprised of a linear combination of a doublet spectrum (blue lines) and a triplet spectrum (orange lines). The corresponding simulation parameters are displayed in table 1.

The resolution of this conundrum was only reached after analysing the pulse ESR results (see below). The conclusion is that the **FAAF** spectra in figure 3 do indeed arise from a *mixture* of a doublet component, akin to **AAF**, and a triplet component (see also table 1). The doublet component tends to dominate the spectra with a weighting of 50-90%. Importantly, its exact weighting is not reproducible between different samples; it is non-trivially dependant on preparation conditions. In the SI, we explore further the effects of different parameters (oxygen, solvent, light, temperature, storage times) on the appearance of the spectra and on the relative weighting of the doublet and triplet components. Although the results are not conclusive, the doublet component observed in liquid solutions of **FAAF** is likely caused by a combination of the following: (1) interactions with molecular oxygen, (2) interactions with light, (3) interactions with the solvent, and (4) intermolecular interactions (*e.g.* π-stacking). All these factors are also consitent with a degradation of the triplet state to another fluorenyl-based doublet species. Although the doublet/triplet ratio is not reproducible, the hyperfine couplings of the two components are persistently the same between different samples, preparation methods, and storage times. Importantly, all the hyperfine couplings of the triplet component are approximately half of those in the doublet component. As discussed in

4

the SI, this halving of the hyperfine interaction in the triplet is reproduced by the DFT results and it can also be explained intuitively by invoking the Pauli exclusion principle.

2.2 Pulse ESR

Whilst compelling, the arguments of the previous section rely on two leaps-of-faith. Firstly, one has to accept that the spectrum of **FAAF** is a superposition of a doublet and triplet component and secondly, one has to trust that the 30 parameter cwESR fitting results are unique. The first independent piece of evidence in support of the doublet-triplet admixture comes from the free induction decay (FID) spectra in figure 4 and the associated simulation parameters in table 2. Whilst for cwESR, the difference between **AAF** and **FAAF** was clearest when examining the ^{13}C–labelled spectra, the unlabelled species offer the best comparison of the FID spectra of frozen solutions. In frozen solutions, the significant anisotropy of the ^{13}C hyperfine tensor masks the fine-structure of the triplet component of **FAAF**. The FID spectra of the ^{13}C labelled species are shown in the SI, together with the results of hyperfine sub-level correlation spectroscopy which validates our claim about the significant anisotropy of the ^{13}C coupling. Therefore, the remaining analysis will focus only on the unlabelled species.
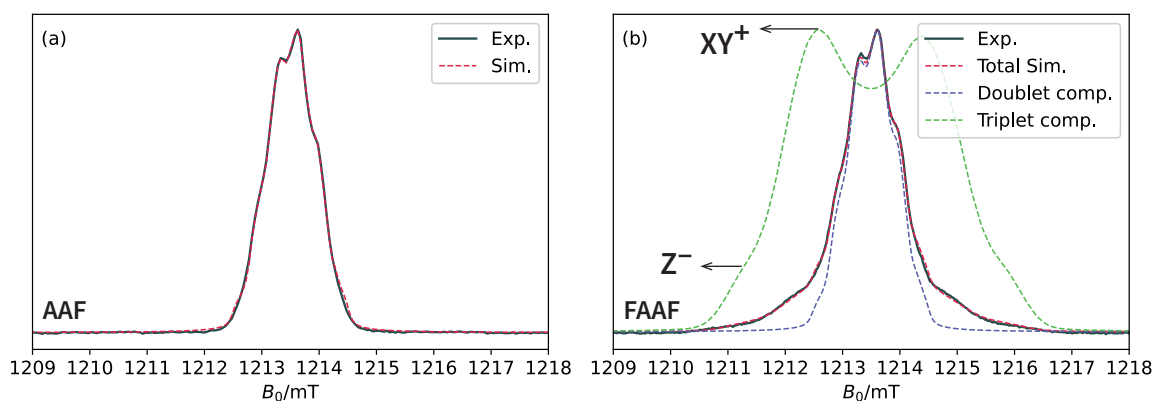

Figure 4: (a) FID field swept experimental and simulated spectrum of **AAF** recorded at 80 K and Q-band using deuterated toluene as the solvent. (b) Experimental and simulated FID spectrum of the **FAAF** system. The simulation was achieved with a doublet/triplet weighting of 85%/15%. A summary of the simulation parameters is shown in table 2; full simulation scripts are in the SI. For the triplet component of **FAAF** the anisotropy of the dipolar interaction, *i.e.* the **D**-tensor, is responsible for the Pake pattern appearance of the dashed green spectrum in panel (b). The turning points on the left of the spectrum are labelled as Z^- and XY^+ (the corresponding labels on the right of the spectrum would be Z^+ and XY^-). The Z label represents resonance fields corresponding to molecules for which the D_z-axis of the **D**-tensor is parallel to the external magnetic field, whereas the XY label refers to molecules with D_z perpendicular to the magnetic field. The superscripts, $\pm$, correspond to the $T_- \rightarrow T_0$ and $T_0 \rightarrow T_+$ electron spin transitions, respectively.

The interpretation of the **AAF** FID data is simple: the spectrum is modelled excellently by four almost equivalent proton hyperfines of ca. 10 MHz. The slight asymmetry of the spectrum relative to its barycentre is most easily quantified by a slightly anisotropic **g**-tensor (table 2). However, the FID spectrum of **FAAF** is now clearly distinct from **AAF**. The triplet component appears as the broad shoulders to either side of the central doublet component which is otherwise akin to **AAF**. Similarly to cwESR, the weighting of the doublet is dominant (85% in this particular case). Yet, as for the cwESR data, the doublet weighting is not consistently the same between different samples. Nonetheless, all other simulation parameters remain reproducible. Particularly comforting is the fact that the halving of the triplet hyperfine couplings observed in the cwESR data is also reproduced in the FID data. The biggest difference between the liquid solution cwESR and frozen solution FID spectra comes from the fact that the anisotropy of the dipolar coupling of the triplet component is resolved in the latter. This interaction is responsible for the $Z^\pm$ and $XY^\pm$ turning points depicted in panel (b) of figure 4. As shown in the SI, the spacing between the Z^- and Z^+ turning points of the triplet component is equivalent to $2|D|$, where D is the dipolar coupling (related to the maximum, D_z, eigenvalue of the dipolar coupling tensor by $D = (3/2)D_z$). The sign of D was chosen to be negative in these simulations, in keeping with the prolate spin density of **FAAF**. The magnitude of D is related to the average interspin distance between the two unpaired electrons of **FAAF**. A 'back-of-the-envelope' calculation, based on the simplified formula: $|D| \approx 490 \text{ nm}^3 \text{ MHz}/\langle r \rangle^3$, predicts an average interspin distance $\langle r \rangle \approx 1.89 \text{ nm}$. This estimated distance is consistent with the DFT optimised geometry for the gas phase structure of **FAAF** which has a distance of 1.8964 nm between the centres of the fluorenyl (**F**) fragments. Extracting $\langle r \rangle$ in this simplified manner may lead to discrepancies caused by the exchange-type integrals contributing to the D-value (this is *not* the exchange interaction, J).[25] A better estimate of the dipolar

FAAF – doublet		FAAF – triplet		AAF	
Parameter	Value	Parameter	Value	Parameter	Value
$a_{iso}(4\times{}^1H)$/ MHz	10.2	$a_{iso}(8\times{}^1H)$/ MHz	4.9	$a_{iso}(4\times{}^1H)$/ MHz	10.2
σ_L/mT	0.10	σ_L/mT	0.10	σ_L/mT	0.10
σ_G/mT	0.08	σ_G/mT	0.08	σ_G/mT	0.08
g_1	2.00231	g_1	2.00240	g_1	2.00226
g_2	2.00172	g_2	2.00119	g_2	2.00170
g_3	2.00136	g_3	2.00170	g_3	2.00131
–	–	D/MHz	-72 MHz	–	–

Table 2: Simulation parameters used to obtain the results in figure 4. For **FAAF**, the spectrum was simulated using an 85% triplet component. The spectra were simulated by employing isotropic proton hyperfine couplings and an anisotropic **g**-tensor with eigenvalues g_1, g_2, and g_3. The dipolar coupling of the triplet component of **FAAF** was taken into account via the D-value. Simulations with anisotropic hyperfine couplings were also attempted, however, the number of parameters is very large and renders the interpretation meaningless. It is clear that the asymmetry of the experimental FID spectra is modelled accurately only by the anisotropy of the **g**-tensor.

interaction is provided by calculating the D-value using the DFT spin density. Such a calculation predicts that $D = -67.5$ MHz which is comparable to the experimental value of -72 MHz with a strain of ±5 MHz.

While the analysis of the FID spectra is more convincing than cwESR regarding the presence of a doublet/triplet admixture in solutions of **FAAF**, there is still a need for an experiment which proves conclusively and without relying on multi-parameter simulations that this admixture is truly present. Given that the admixture is already 'suspected', the experimental test is trivial: the nutation frequencies of the two components should be related by a factor of $\sqrt{2}$ (see SI). This effect is clearly observed in the nutation data presented in the SI, thus validating the conclusions from both cwESR and FID experiments.
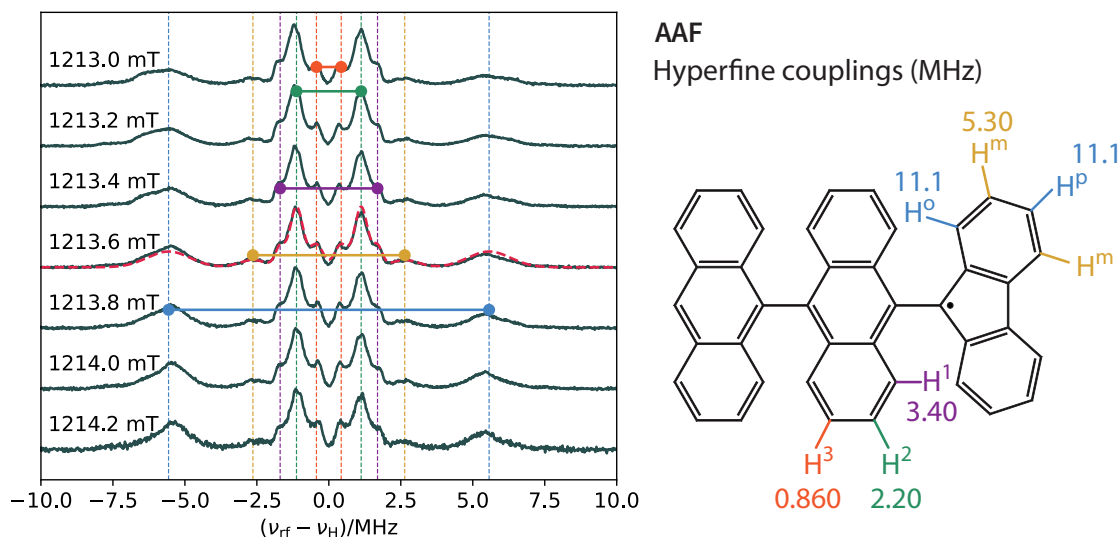
Figure 5: One-dimensional Mims ENDOR spectra of **AAF** recorded across the ESR spectrum starting from 1213.0 mT in steps of 0.2 mT. The maximum in the ESR spectrum (see figure 4) corresponds to the ENDOR spectrum at 1213.6 mT. The dashed red line superimposed on the 1213.6 mT data represents the best-fitting of a sum of 5 symmetric bimodal Gaussian functions. The centres of the bimodal Gaussians are denoted by the coloured circles; the gaps between these circles correspond to the magnitudes of the hyperfine couplings. These couplings are assigned to the protons of the **AAF** molecules as depicted by the colours in the skeletal structure on the right. The assignment was done by comparison of the experimental values with the DFT computed hyperfine tensors.

One of the reasons why the nutation experiment mentioned above was successful is that solutions of **FAAF** contain a doublet-triplet admixture which allows the nutation frequencies to be compared. However, in general

terms, this method would not work if the sample contained species with the same total spin quantum number. The nutation experiment requires a reference frequency. Such a reference may be obtained either by a precise calibration of the microwave power or the deliberate mixing of a species with known spin quantum number into the unknown sample. These methods are both cumbersome and prone to errors. Below we propose and deploy a more versatile method, based on ENDOR, which can be used to disentangle the spin states present in liquid solutions of multi-radical systems.

2.3 Electron nuclear double resonance

Figures 5 and 6 summarise the 1D-ENDOR results for **AAF** and **FAAF**. These ENDOR spectra were acquired across the ESR spectrum using microwave pulse lengths of 54 ns with a bandwidth of ca. 22 MHz (0.8 mT in field domain). For **AAF**, this pulse bandwidth is responsible for the small orientation selection effects observed in the ENDOR spectra acquired at different field positions. Apart from these small differences, the **AAF** ENDOR spectra are symmetric relative to the Larmor frequency ($\nu_{rf} - \nu_H = 0$), as expected for a doublet. The observed peaks are assigned to particular protons in **AAF** by performing a Gaussian deconvolution and comparing the results with the DFT predicted hyperfine tensors. As was the case for all data up to this point, the largest hyperfine coupling (blue line in figure 5) corresponds to the *ortho/para* protons marked in the skeletal structures. The smaller hyperfine couplings to the *meta* protons and the anthryl protons are also clearly resolved in the data.
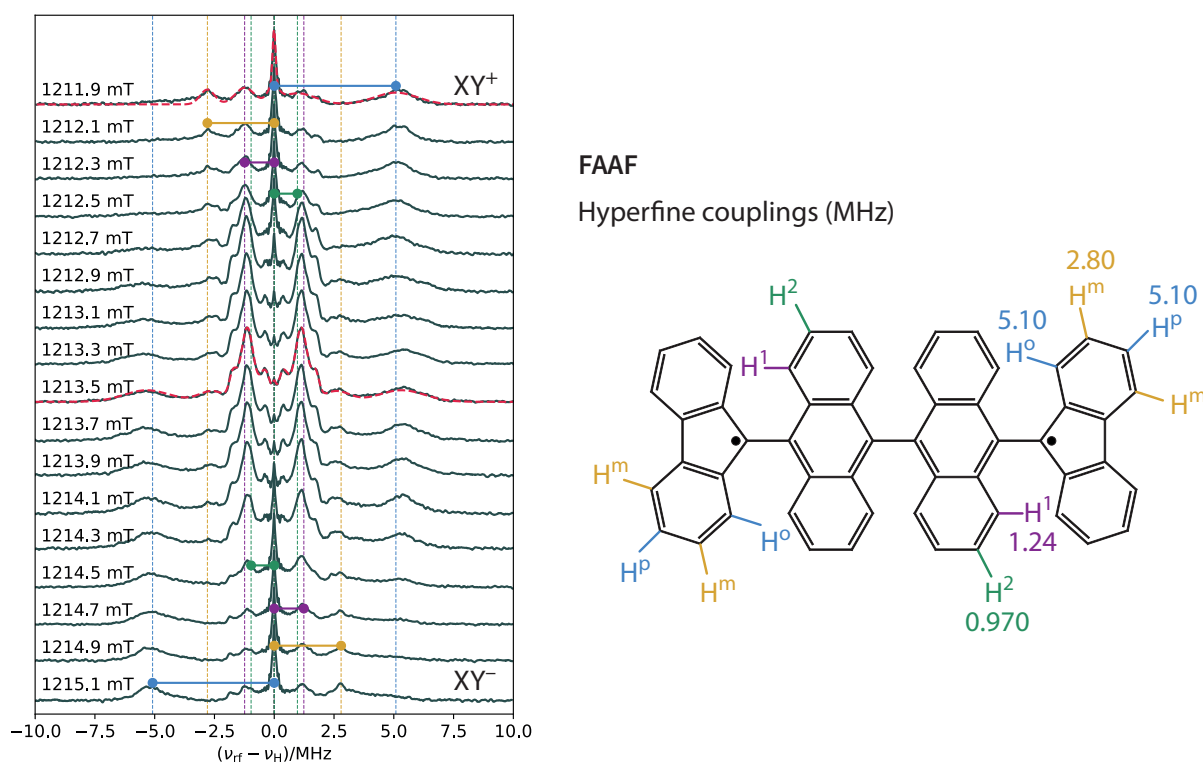
Figure 6: One-dimensional Mims ENDOR spectra of **FAAF** recorded across the ESR spectrum. The maximum in the ESR spectrum (see figure 4) corresponds to the ENDOR spectrum at 1213.5 mT. The dashed red line superimposed on the 1213.5 mT data represents the best-fitting of a sum of 5 symmetric bimodal Gaussian functions. By contrast, the dashed red line superimposed on the 1211.9 mT data represents the best-fitting of a sum of 5 ('single mode') Gaussian functions. Similarly to figure 5, the hyperfine couplings were assigned to the protons of **FAAF** by comparison with the DFT results. At the central field positions (1212.7–1214.3 mT), the ENDOR spectra of **FAAF** are very similar to the **AAF** (except for the appearance of the Larmor peak). However, the peripheral spectra, corresponding to the shoulders observed in the **FAAF** spectrum in figure 4, are strongly indicative of a triplet state (strong Larmor peak and pronounced asymmetry). As mentioned in the SI, the sign of the hyperfine coupling can be determined for triplet states if the sign of the D-value is known. The data shows that the *ortho/para* protons have a negative hyperfine coupling (*i.e.* an excess of β spin density) and the *meta* protons have a positive hyperfine coupling (*i.e.* an excess of α spin density). These relative signs are entirely reproduced by the phase of the DFT computed spin density.

By contrast with **AAF**, the ENDOR spectra of **FAAF** (figure 6) depend strongly on field position. At the low-field side, the *ortho/para* protons give rise to a single peak centred at +5 MHz. The *meta* protons produce the peak

7
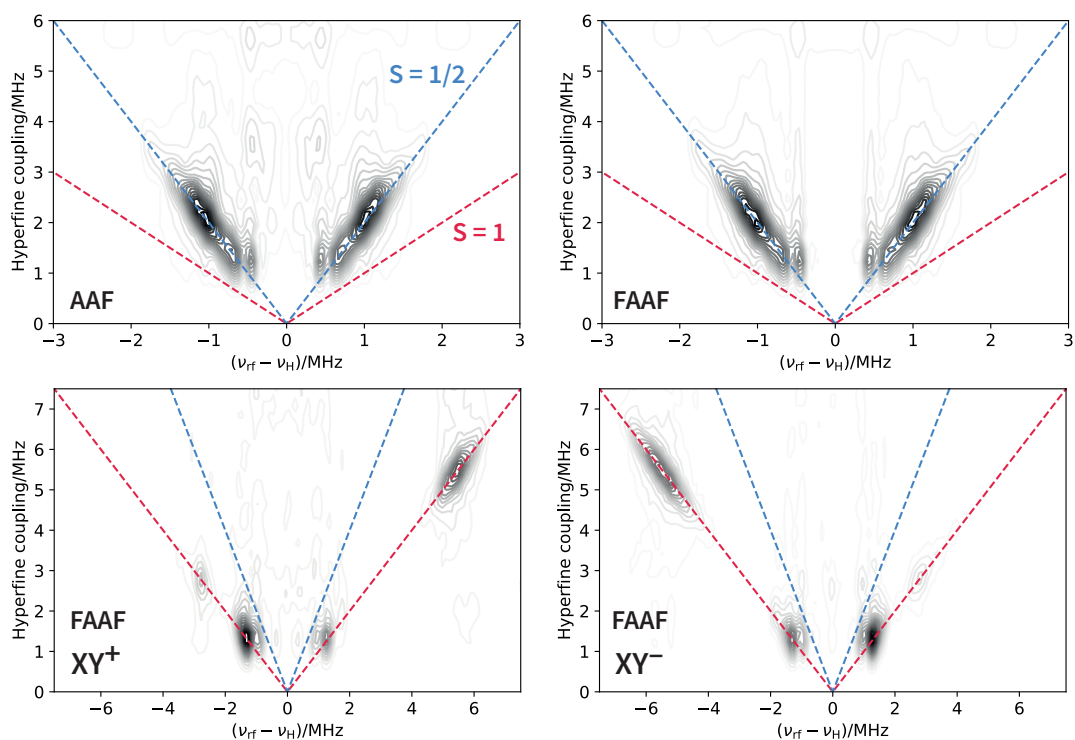
Figure 7: Hyperfine-correlated ENDOR results for **AAF** and **FAAF**. (Top left) Data obtained at the central field position (1213.6 mT) of the **AAF** FID spectrum. The correlation ridges are observed along the dashed blue $S = 1/2$ line corresponding to a hyperfine coupling equal to $2|\nu_{rf} - \nu_H|$. (Top right) Data collected at the central field position of the **FAAF** FID spectrum (1213.5 mT). (Bottom left/right) Data collected on the two left/right shoulders of the **FAAF** FID spectrum at 1211.9 and 1215.1 mT, respectively. The correlation ridges are along the dashed red $S = 1$ line corresponding to hyperfine coupling magnitudes equal to $|\nu_{rf} - \nu_H|$. The mirror image symmetry between the two panels originates in the same effect as discussed for the 1D ENDOR spectra.

at -2.5 MHz. As the field position approaches the centre of the ESR spectrum, the ENDOR data becomes more symmetric relative to the Larmor frequency. At the centre fields (1212.9 mT – 1214.1 mT), the **FAAF** spectra are effectively identical to **AAF** (apart from the Larmor peak). As the high-field side of the ESR spectrum is approached, the ENDOR spectra become almost perfect mirror images of the corresponding low-field spectra. As explained in the SI, the presence of the Larmor peak and the mirror image symmetry of the low/high-field ENDOR spectra are signatures of a triplet state. The only problem is the similarity of the **FAAF** and **AAF** data at the centre fields. In the absence of other evidence, the data at 1213.5 mT would be consistent *both* with a doublet/triplet admixture and with a *pure* triplet state. This is because, when the anisotropy of the dipolar coupling is taken into account, both triplet transitions $T_0 \to T_+$ and $T_0 \to T_-$ are excited at the centre field position (*i.e.* at the mid-point between XY^+ and XY^- – figure 4 – corresponding to an angle of 54.7° between D_z and the magnetic field).

Hence, a pure triplet ENDOR spectrum recorded at the centre field would contain a Larmor peak and hyperfine peaks on either side of it, as would the ENDOR spectrum of a doublet/triplet admixture. Nonetheless, we already know from all the previously presented results that the admixture is truly the origin of the similarity between the ENDOR spectra of **AAF** and **FAAF** at the centre field position. However, in more complicated systems, such clear spectral simulations and nutation experiments are the exception, not the rule. In those circumstances, how could we test, experimentally, whether the 1213.5 mT ENDOR spectrum in figure 6 is caused by a doublet/triplet admixture or a pure triplet? The answer lies in the hyperfine-correlated ENDOR experiment shown in figure 7. As explained in the SI, hyperfine-correlated ENDOR produces 2D spectra where the peaks in the usual 1D-ENDOR spectra are correlated with the hyperfine couplings from which they originate. A doublet electronic spin coupled to multiple protons will give rise to hyperfine correlation ridges along the $2|\nu_{rf} - \nu_H|$ line in the hyperfine dimension. This line is shown in dashed blue in figure 7. For **AAF**, the data in the top left panel is fully consistent with an electronic spin quantum number of 1/2. When the measurement is performed on the central field position of the **FAAF** spectrum, the result is effectively identical to **AAF**. A triplet electronic spin produces hyperfine correlation ridges along the $|\nu_{rf} - \nu_H|$ line (dashed red in figure 7). The bottom panels in figure 7 show that the assignment of a triplet state to the shoulders in the pulse ESR spectra of **FAAF** is correct. Overall, the hyperfine-correlated ENDOR experiment demonstrates uniquely, without relying on subjective interpretation, overly parametrised simulations, and external references with known S, that solutions of the **FAAF** diradical

contain a mixture of doublet and triplet species.

It is worth mentioning other advantages of using hyper-fine-correlated ENDOR to assign the electronic spin quantum number. The technique achieves a frequency discrimination between two multiplets which is proportional to the ratio of the magnetic quantum numbers M_{S_1} and M_{S_2} involved in an ENDOR transition. This is because the hyperfine field experienced by a nucleus is proportional to the magnetic quantum numbers. For doublets *vs.* triplets, this simply implies a frequency discrimination factor of 2 (illustrated by the dashed red/blue lines in figure 7). By contrast, the nutation experiment (SI) achieves, at best, a frequency discrimination factor of $\sqrt{2}$ between doublets and triplets. Moreover, unlike nutation experiments, hyperfine-correlated ENDOR is not subject to distortions caused by microwave field inhomogeneities or complications due to the limited excitation bandwidth of the microwave pulses.

3 Conclusion

The most important result of this work is a quantitative experimental solution to the problem of classifying the electronic spin state of organic diradicals by ESR spectroscopy. The rich ESR behaviour observed for these particular Chichi-babin radicals, **AAF** and **FAAF**, has allowed such a solution to be developed systematically. To start with, a quantitative analysis of the liquid state cwESR spectra provided the first hint that liquid solutions of **FAAF** contain a mixture of species with different spin quantum numbers (doublets and triplets). In fact, the doublet component only appears distinctly in the ESR spectra and cannot be conclusively gleaned from the other characterisation techniques used in the synthesis (see SI). Further and clearer evidence supporting the presence of this admixture was obtained from analysing the FID spectra, the nutation spectra, and one-dimensional ENDOR data. However, the technique which offered the most direct discrimination between the two components proved to be hyperfine-correlated ENDOR. This latter experiment relies only on the nuclear spins acting as reporters of the electronic spin quantum numbers. The interpretation of the hyperfine-correlated ENDOR data in figure 7 does not require overly parameterised simulations, or an external reference for the spin quantum number. It is therefore applicable to a wider array of PAHs, and other species, with unpaired electrons, beyond **FAAF** and **AAF**.

The doublet component present in solutions of **FAAF** is a fluorenyl-based monoradical, akin to **AAF**, arising from a non-trivial interplay of many variables, such as: interactions with molecular oxygen, with other molecules of the same type, with the solvent, and with light. However, it is now clear that the 'doublet impurity' noted by researchers working on these and similar systems for the past 53 years is, perhaps, not an impurity at all. [26–29]

Acknowledgements

Conflicts of interest declaration

The authors have no conflicts of interest to declare.

References

[1] R. G. Harvey. *Polycyclic aromatic hydrocarbons.* Wiley, New York, 1997.

[2] Z. Zeng, X. Shi, C. Chi, J. T. L. Navarrete, Ju. Casado, and J. Wu. Pro-aromatic and anti-aromatic π-conjugated molecules: an irresistible wish to be diradicals. *Chem. Soc. Rev.*, 44(18):6578–6596, 2015.

[3] M. Abe. Diradicals. *Chem. Rev.*, 113(9):7011–7088, 2013.

[4] Kenji Kamada, Koji Ohta, Takashi Kubo, Akihiro Shimizu, Yasushi Morita, Kazuhiro Nakasuji, Ryohei Kishi, Suguru Ohta, Shin-ichi Furukawa, Hideaki Takahashi, and Masayoshi Nakano. Strong two-photon absorption of singlet diradical hydrocarbons. *Angew. Chem. Int. Edit.)*, 46(19):3544–3546, 2007.

[5] Kevin M Felter and Ferdinand C Grozema. Singlet fission in crystalline organic materials: Recent insights and future directions. *J. Phys. Chem. Lett.*, 10(22):7208–7214, 2019.

[6] Paula Mayorga-Burrezo, Vicente G Jiménez, Davide Blasi, Teodor Parella, Imma Ratera, Araceli G Campaña, and Jaume Veciana. An enantiopure propeller-like trityl-brominated radical: Bringing together a high racemization barrier and an efficient circularly polarized luminescent magnetic emitter. *Chem.-Eur. J.*, 26(17):3776–3781, 2020.

[7] Qingxian Jin, Sanxu Chen, Yutao Sang, Haoqing Guo, Shengzhi Dong, Jianlei Han, Wenjie Chen, Xuefeng Yang, Feng Li, and Pengfei Duan. Circularly polarized luminescence of achiral open-shell π-radicals. *Chem. Commun.*, 55(46):6583–6586, 2019.

[8] Masayuki Chikamatsu, Takefumi Mikami, Jiro Chisaka, Yuji Yoshida, Reiko Azumi, Kiyoshi Yase, Akihiro Shimizu, Takashi Kubo, Yasushi Morita, and Kazuhiro Nakasuji. Ambipolar organic field-effect transistors based on a low band gap semiconductor with balanced hole and electron mobilities. *Appl. Phys. Lett.*, 91(4), 2007.

[9] Zhe Sun and Jishan Wu. Open-shell polycyclic aromatic hydrocarbons. *J. Mater. Chem.*, 22(10):4151–4160, 2012.

[10] Yasushi Morita, Shuichi Suzuki, Kazunobu Sato, and Takeji Takui. Synthetic organic spin chemistry for structurally well-defined open-shell graphene fragments. *Nat. Chem.*, 3(3):197–204, 2011.

[11] Federico Lombardi, Alessandro Lodi, Ji Ma, Junzhi Liu, Michael Slota, Akimitsu Narita, William K Myers, Klaus Müllen, Xinliang Feng, and Lapo Bogani. Quantum units from the topological engineering of molecular graphenoids. *Science*, 366(6469):1107–1110, 2019.

[12] Junzhi Liu and Xinliang Feng. Synthetic tailoring of graphene nanostructures with zigzag-edged topologies: progress and perspectives. *Angew. Chem. Int. Edit.*, 59(52):23386–23401, 2020.

[13] Wangdong Zeng and Jishan Wu. Open-shell graphene fragments. *Chem*, 7(2):358–386, 2021.

[14] Shaotang Song, Jie Su, Mykola Telychko, Jing Li, Guangwu Li, Ying Li, Chenliang Su, Jishan Wu, and Jiong Lu. On-surface synthesis of graphene nanostructures with π-magnetism. *Chem. Soc. Rev.*, 50(5):3238–3262, 2021.

[15] ZX Chen, Y Li, and F Huang. Persistent and stable organic radicals: Design, synthesis, and applications. *Chem*, 7(2):288–332, 2021.

[16] Tao Wang, Sofia Sanz, Jesús Castro-Esteban, James Lawrence, Alejandro Berdonces-Layunta, Mohammed SG Mohammed, Manuel Vilas-Varela, Martina Corso, Diego Peña, Thomas Frederiksen, and Dimas G. de Oteyza. Magnetic interactions between radical pairs in chiral graphene nanoribbons. *Nano Lett.*, 22(1):164–171, 2021.

[17] Yuan Li, Wee-Kuan Heng, Byung Sun Lee, Naoki Aratani, José L Zafra, Nina Bao, Richmond Lee, Young Mo Sung, Zhe Sun, Kuo-Wei Huang, Richard D. Webster, Juan T. López Navarrete, Dongho Kim, Atsuhiro Osuka, Juan Casado, Jun Ding, and Jishan Wu. Kinetically blocked stable heptazethrene and octazethrene: closed-shell or open-shell in the ground state? *J. Am. Chem. Soc.*, 134(36):14913–14922, 2012.

[18] Niko Pavliček, Anish Mistry, Zsolt Majzik, Nikolaj Moll, Gerhard Meyer, David J Fox, and Leo Gross. Synthesis and characterization of triangulene. *Nat. Nanotechnol.*, 12(4):308–311, 2017.

[19] Shantanu Mishra, Shadi Fatayer, Saleta Fernández, Katharina Kaiser, Diego Peña, and Leo Gross. Nonbenzenoid high-spin polycyclic hydrocarbons generated by atom manipulation. *ACS Nano*, 16(2):3264–3271, 2022.

[20] A. E. Chichibabin. Über einige phenylierte Derivate des p, p-Ditolyls. *Chem. Ber.*, 40:1810, 1907.

[21] Z. Zeng, Y. M. Sung, N. Bao, D. Tan, R. Lee, J. L. Zafra, B. S. Lee, M. Ishida, J. Ding, J. T. L. Navarrete, Y. Li, W. Zeng, D. Kim, K.-W. Huang, R. D. Webster, J. Casado, and J. Wu. Stable tetrabenzo-chichibabin's hydrocarbons: tunable ground state and unusual transition between their closed-shell and open-shell resonance forms. *J. Am. Chem. Soc.*, 134(35):14513–14525, 2012.

[22] Zhenglong Lim, Bin Zheng, Kuo-Wei Huang, Ye Liu, and Jishan Wu. Quinoidal oligo (9, 10-anthryl) s with chain-length-dependent ground states: A balance between aromatic stabilization and steric strain release. *Chem.-Eur. J.*, 21(51):18724–18729, 2015.

[23] Vicente G Jiménez, Paula Mayorga-Burrezo, Victor Blanco, Vega Lloveras, Carlos J Gómez-García, Tomáš Šolomek, Juan M Cuerva, Jaume Veciana, and Araceli G Campana. Dibenzocycloheptatriene as end-group of thiele and tetrabenzo-chichibabin hydrocarbons. *Chem. Commun.*, 56(84):12813–12816, 2020.

[24] Thomas Y Baum, Saleta Fernández, Diego Peña, and Herre SJ Van Der Zant. Magnetic fingerprints in an all-organic radical molecular break junction. *Nano Lett.*, 22(20):8086–8092, 2022.

[25] S. Sinnecker and F. Neese. Spin- spin contributions to the zero-field splitting tensor in organic triplets, carbenes and biradicals a density functional and ab initio study. *J. Phys. Chem. A*, 110(44):12267–12275, 2006.

[26] Justin J Dressler, Zheng Zhou, Jonathan L Marshall, Ryohei Kishi, Shota Takamuku, Zheng Wei, Sarah N Spisak, Masayoshi Nakano, Marina A Petrukhina, and Michael M Haley. Synthesis of the unknown indeno [1, 2-a] fluorene regioisomer: Crystallographic characterization of its dianion. *Angew. Chem. Int. Edit.*, 56 (48):15363–15367, 2017.

[27] T. Nishiuchi, S. Aibara, H. Sato, and T. Kubo. Synthesis of π-extended Thiele's and Chichibabin's hydrocarbons and effect of the π-congestion on conformations and electronic states. *J. Am. Chem. Soc.*, 144(16): 7479–7488, 2022.

[28] W. J. Van der Hart and L. J. Oosterhoff. The ESR and electronic absorption spectra of Chichibabin's biradical. *Mol. Phys.*, 18(2):281–284, 1970.

[29] F. Popp, F. Bickelhaupt, and C. Maclean. The electronic structure of Chichibabin's hydrocarbon. *Chem. Phys. Lett.*, 55(2):327–330, 1978.